Sub-ballistic growth of Rényi entropies due to diffusion

Tibor Rakovszky,[1] Frank Pollmann,[1] and C.W. von Keyserlingk[2]

[1] *Department of Physics, T42, Technische Universität München, James-Franck-Straße 1, D-85748 Garching, Germany*

[2] *University of Birmingham, School of Physics & Astronomy, B15 2TT, UK*

We investigate the dynamics of quantum entanglement after a global quench and uncover a qualitative difference between the behavior of the von Neumann entropy and higher Rényi entropies. We argue that the latter generically grow *sub-ballistically*, as $\propto \sqrt{t}$, in systems with diffusive transport. We provide strong evidence for this in both a U(1) symmetric random circuit model and in a paradigmatic non-integrable spin chain, where energy is the sole conserved quantity. We interpret our results as a consequence of local quantum fluctuations in conserved densities, whose behavior is controlled by diffusion, and use the random circuit model to derive an effective description. We also discuss the late-time behavior of the second Rényi entropy and show that it exhibits hydrodynamic tails with *three distinct power laws* occurring for different classes of initial states.

Introduction.— The far-from-equilibrium dynamics of closed quantum many-body systems has been at the center of much recent attention, both theoretically and experimentally [1–5]. In systems where the Eigenstate Thermalization Hypothesis (ETH) [3, 6, 7] holds, the density matrix, ρ_A, of a finite subsystem relaxes to a Gibbs state with an extensive entropy that stems from the entanglement with the rest of the system, making the dynamics of entanglement integral to the understanding of equilibration. This question has recently become amenable to experimental probes in systems of cold atoms, through the measurement of *Rényi entropies* $S_\alpha \equiv \frac{1}{1-\alpha}\log \mathrm{tr}(\rho_A^\alpha)$, The theoretically most relevant of these is the *von Neumann entropy*, $S_{\alpha\to 1} \equiv -\mathrm{tr}(\rho_A \log \rho_A)$. Experimentally, however, for large subsystems only entropies with integer $\alpha \geq 2$ are currently accessible [5, 8–11]. It is therefore important to understand how their behavior might differ from that of S_1.

In generic clean systems, the von Neumann entropy is expected to grow linearly in time for approximately homogeneous initial states ('global quenches'). This is understood for integrable systems from a quasi-particle description [12–15], but it also holds for thermalizing models [16], where it has recently been described using a 'minimal cut' picture [17–19]. A generic linear growth of S_2 was also proposed in Refs. 20 and 21, based on ballistic spreading of operators, and confirmed in a variety of models with no conservation laws [22–25]. Here we argue that this picture changes drastically in systems exhibiting diffusive transport of some conserved quantity (spin, charge, energy, etc.) [26–28]: we find that $S_{\alpha\geq 2}$ grows *diffusively*, as $\sqrt{t}$. This arises because entropies with $\alpha \geq 2$ are sensitive to the presence of a few anomalously large eigenvalues of the reduced density matrix, while S_1 is dominated by the many exponentially small eigenvalues. The possibility of such a qualitative difference was discussed for global cat states in Ref. 18; here we propose that it arises much more generally, without the need to fine tune the initial state.

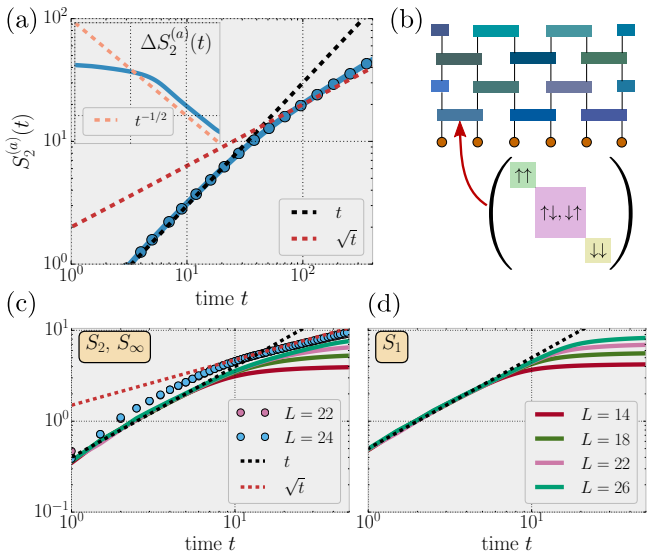

FIG. 1. (a) Growth of (annealed average) second Rényi entropy in a spin 1/2, U(1)-symmetric random circuit, averaged over all product states. At long times the growth is diffusive ($\propto \sqrt{t}$). Inset: the discrete time derivative $\Delta S_2^{(a)}(t) \equiv S_2^{(a)}(t+1) - S_2^{(a)}(t)$ decays as $t^{-1/2}$. (b) Geometry of the random circuit and block structure of the gates. (c): Rényi entropies of the tilted field Ising model (1), S_2 (solid lines) and S_∞ (dots) show a similar cross-over to sub-ballistic growth, while (d) the von Neumann entropy grows mostly linearly.

Numerical results.— We consider a local random unitary circuit with a conserved U(1) charge as a simple toy model of local quantum dynamics with diffusive transport [29, 30]. We take a spin 1/2 chain and evolve it with 2-site unitary gates that are block-diagonal in the total z-spin (see Fig. 1b). Each unitary consists of three independent Haar random blocks, corresponding to the states $\{\uparrow\uparrow\}$, $\{\uparrow\downarrow, \downarrow\uparrow\}$, $\{\downarrow\downarrow\}$. In every time step we apply such two-site gates first on all even, then on all odd bonds of the chain, and the different gates in the circuit are all independently chosen. Clearly, this circuit conserves the

total Pauli z component, $\sum_x Z_x$.

We examine the circuit-averaged purity $\overline{\mathcal{P}}$, where the purity is $\mathcal{P} \equiv e^{-S_2} = \mathrm{tr}(\rho_A^2)$. This defines the *annealed average* Rényi entropy, $S_2^{(a)} \equiv -\log \overline{\mathcal{P}}$, which lower bounds the average Rényi entropy, $\overline{S_2} \geq S_2^{(a)}$. $\overline{\mathcal{P}}$ is represented as a classical partition function using the mapping derived in Ref. 30, which we now evaluate using standard tensor network methods [31, 32], making sure that the results are converged both in system size and bond dimension. Moreover, we average over all initial product states exactly. As shown in Fig. 1a, we find an entanglement growth of the form $S_2^{(a)} \propto \sqrt{t}$ at long times. Note that the same quantity would grow linearly if we removed the conservation law [22, 23], thus we attribute its slow growth to diffusive transport. This is one of our central results.

Next, we consider the spin 1/2 Hamiltonian

$$H = J \sum_{r=1}^{L-1} Z_r Z_{r+1} + \sum_{r=1}^{L} (h_z Z_r + h_x X_r) - J(Z_1 + Z_L), \quad (1)$$

where the last term is included to decrease boundary effects. We refer to (1) as the *tilted field Ising model*. We choose $J = 1$, $h_x = (5+\sqrt{5})/8$, and $h_z = (1+\sqrt{5})/4$, as the same model was previously shown to have diffusive energy transport and linear von Neumann entropy growth [16]. Fig. 1c,d show the growth of different entropies, averaged over $N = 50$ random product states for system sizes $L = 12 - 24$ and $N = 20$ for $L = 26$. We observe a mostly linear growth of S_1, in agreement with Ref. 16. However, looking at S_2 we find that it has a cross-over to a sub-linear growth at the longest times. Although the times we can investigate are limited by finite system size, the long-time behavior is consistent with $\propto \sqrt{t}$ growth. The results become more clear if we consider the *min-entropy*, $S_{\alpha\to\infty}$ which provides an upper bound on $S_{\alpha\geq 2} \leq 2S_\infty$. We find that S_∞ is less sensitive to finite size effects, and also exhibits a more pronounced cross-over towards $\sqrt{t}$ growth (see dots in Fig. 1c). Similar results hold also for particular initial states, without averaging [33]. The behavior of the random circuit and Hamiltonian models leads us to conjecture that such diffusive growth of $S_{\alpha\geq 2}$ is a generic consequence of diffusive hydrodynamic transport. In the following we provide further justification of this conjecture.

Heuristic argument.— We interpret our results in terms of the following non-rigorous argument. Let us focus on a Z-conserving discrete time evolution, $U(t) = \prod_{\tau<t} U(\tau, \tau+1)$ on an infinite chain and consider the bipartite entanglement at a cut between sites x and $x+1$. We can rewrite the time evolved state as a 'sum over histories', $|\psi(t)\rangle = U(t)|\psi_0\rangle = \sum_{\{\sigma(\tau)\}} A(\{\sigma(\tau)\})|\sigma\rangle$, where $A(\{\sigma(\tau)\})$ is a probability amplitude associated to a world history $\{\sigma(\tau)\}|_{0\leq\tau\leq t}$ in the Z basis. We split this sum into two parts: i) world histories for which the the sites $x, x+1$ have both spins up at all times $\tau > t_{\mathrm{loc}}$ for some local equilibration time $t_{\mathrm{loc}} \sim \mathcal{O}(1)$, and ii) all remaining paths. Let $|\phi_0(t)\rangle$ and $|\phi_1(t)\rangle$ denote the normalized states corresponding to these two sums over paths. Then $|\psi\rangle = c_0|\phi_0\rangle + c_1|\phi_1\rangle$, where we have dropped the explicit t dependence. While in general, calculating the entanglement of such a superposition is a difficult task, it simplifies when $|\phi_{1,2}\rangle$ are *biorthogonal*, meaning they are completely distinguishable from each other by measurements on just one side of the entanglement cut [34]. In this case, the bipartite entropies, S_1 and S_2, of $|\psi\rangle$ can be calculated explicitly [35–37]:

$$\begin{aligned} S_1[\psi] &= |c_0|^2 S_1[\phi_0] + |c_1|^2 S_1[\phi_1] + h_2(|c_0|^2) \\ e^{-S_2[\psi]} &= |c_0|^4 e^{-S_2[\phi_0]} + |c_1|^4 e^{-S_2[\phi_1]}, \end{aligned} \quad (2)$$

where $h_2(\lambda) \equiv -\lambda\log(\lambda) - (1-\lambda)\log(1-\lambda) \leq \log 2$ is the binary entropy function.

By construction, $|\phi_0\rangle$ has at most $\mathcal{O}(1)$ entanglement, accumulated by the time t_{loc}. Suppose, moreover, that $S_{1,2}[\phi_1]$ grow as fast as allowed by locality, i.e., linearly in time. We also need to estimate the probability that the sites $x, x+1$ remain in the state $\uparrow\uparrow$ at all times $t > t_{\mathrm{loc}}$. The simplest approximation is to treat every $\downarrow$ in the system as an independently diffusing particle. In this case, the probability that all particles that are to the left of x at t_{loc} remain on the same side is a product of the probabilities for particles starting at different positions. Due to diffusion, the relevant contribution comes from particles that are initially within some region of size $\mathcal{O}(\sqrt{Dt})$ near the entanglement cut, where D is the diffusion constant. Therefore we expect the probability to decay at long times as $|c_0|^2 \propto e^{-\gamma\sqrt{Dt}}$ for some constant γ [38]. Plugging this into Eq. (2) indicates that i) S_1 is dominated by the linearly growing entropy of $|\phi_1\rangle$ up to some small corrections and ii) for e^{-S_2} at long times, the first term, decaying as $e^{-\gamma\sqrt{Dt}}$, always dominates over the second term that decays as e^{-vt}. This implies that at times $t \gg D/v^2$ the Rényi entropy should grow as $S_2 \sim \sqrt{t}$.

The relations (2) rely on the assumption of biorthogonality. While this is an uncontrolled approximation, the result suggests that rare events associated with charge fluctuations can have profound effect on the growth of $S_{\alpha\geq 2}$, making it sub-ballistic. This intuition is further supported by the inequality $S_2 \leq 2S_\infty$, where $S_\infty = -\log \Lambda_{\max}$ depends only on the largest eigenvalue of the reduced density matrix, $\Lambda_{\max}$. Therefore, a single eigenvalue decaying slower than exponentially is sufficient to make the growth of S_2 sub-ballistic. We propose that the aforementioned rare histories provide such a larger than average eigenvalue, provided that all degrees of freedom couple to some conserved charge [39]. In contrast the von Neumann entropy is unconstrained by S_∞, dominated instead by the many exponentially small eigenvalues of ρ_A, leading to linear growth.

While the above argument is presented in the language

of spin conservation, we expect it to generalize to energy conserving systems in the form of rare events where the time evolved state locally resembles the ground state [40]. This is in agreement with our numerical results in Fig. 1c.

Effective model— To get a further analytical handle on this problem, we return to our random circuit model and modify it along the lines of Ref. 29, by adding an extra q-state system to each site, unconstrained by the conservation law. This makes the size of each Haar random unitary larger by a factor of q^2, simplifying calculations in the large q limit, allowing us to derive an effective model that governs the evolution of $S_2^{(a)}$. As we shall see, the result decomposes into the sum of two contributions: a $\propto t$ part from the non-conserved degrees of freedom, and a $\propto \sqrt{t}$ part associated to the conserved spins.

To begin, note that the purity can be written as the expectation value of an operator, by taking two identical copies of the original system [8, 23, 41, 42]. Imagine two copies of a single site, with Hilbert space $\mathcal{H}\otimes\mathcal{H}$, and define the one-site *swap operator* $\mathcal{F}$, such that $\mathcal{F}(|i\rangle\otimes|j\rangle) \equiv |j\rangle\otimes|i\rangle$, where $\{|i\rangle\}$ is a basis in $\mathcal{H}$. Then the half chain purity is $\mathcal{P}(x) = \mathrm{tr}(\mathcal{F}(x)[\rho\otimes\rho]) \equiv \langle\mathcal{F}(x)\rangle$, where $\mathcal{F}(x) \equiv \prod_{\leq x}\mathcal{F}$ is a string of swap operators acting on one half of the entanglement cut (see Fig. 2a,b). Instead of evolving the state, we can alternatively evolve the operator $\mathcal{F}(x)$ in time. Averaging over a random gate on sites $x, x+1$, to leading order in $1/q$ it evolves as [33]

$$\mathcal{F}(x) \to (2q)^{-1}\sum_{y=x\pm1}\mathcal{F}(y) + \tilde{\mathcal{F}}_x(y), \tag{3}$$

where we have introduced new 'two-copy' operators

$$\tilde{\mathcal{F}}_x(y) \equiv (Z_{x,x+1}\otimes Z_{x,x+1})\mathcal{F}(y), \tag{4}$$

with $Z_{x,x+1} \equiv (Z_x + Z_{x+1})/2$, and the tensor product refers to the two copies of the system. These are similar to $\mathcal{F}(x)$, but multiplied by the Z operators that measure the conserved spin on sites near the entanglement cut.

To see how the entanglement evolves, one also needs equations of motion for $\tilde{\mathcal{F}}_x(y)$. This can be done analogously, by averaging over 2-site gates, resulting in the following effective model [33]. We can associate to each Z_x in Eq. (4) a 'particle', with two different colors, red and blue, depending on which of the two copies it acts on [43] (Fig. 2c). Away from the endpoint of the swap-string, these particles independently obey diffusion with hard-core interactions, the number of each species being conserved. The endpoint of the string itself also diffuses, moving one site either to the left or the right, while emitting and absorbing an even number of particles at each step (Fig. 2d). One can show that the probability of emission vs. absorption decreases with the number of particles on the two sites directly at the endpoint, changing sign at half filling. Apart from an overall suppression factor of $2/q$ in each step, this is a Markov process on configurations defined by a string of swap operators ending at some position x', and particle densities

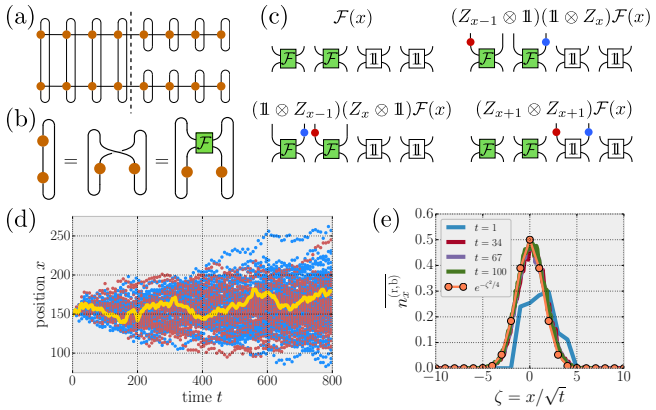

FIG. 2. Effective model at $q\to\infty$. (a) The purity $\mathcal{P}$, written in terms of the state ρ as a matrix product operator. (b) This can be rewritten by introducing the swap operator $\mathcal{F}$. (c) Half-chain 'swap-string' $\mathcal{F}(x)$, along with a few of the terms on the RHS of Eq. (3), with red and blue particles representing local Z_x operators. (d) These particles obey a random walk with hard core interactions, spreading out diffusively, which (e) leads to a Gaussian density profile.

$\{n_y^{(r,b)} = 0, 1\}$; each such configuration corresponds to an operator $\prod_y (Z_y^{n_y^{(r)}}\otimes Z_y^{n_y^{(b)}})\mathcal{F}(x')$.

The swap-string and both types of particles evolve as unbiased random walks, therefore by time t we expect them to occupy a region of width $l(t) = \kappa\sqrt{t}$. Monte Carlo simulations of the stochastic dynamics show (Fig. 2e) that the particle densities are Gaussian around x. We therefore take a mean field approximation and write the probability of a string ending at x and a distribution of particles $\{n_y^{(r,b)} = 0, 1\}$ as

$$p(x, n^{(r)}, n^{(b)}) \propto e^{-\frac{x^2}{2l(t)^2}} e^{-\frac{1}{2l(t)^2}\sum_y (n_y^{(r)}+n_y^{(b)})y^2} \tag{5}$$

if $\sum_y(n_y^{(r)} + n_y^{(b)})$ is even, and zero otherwise. With this ansatz, one can evaluate the half-chain purity at time t. For translation invariant product states, the result reads

$$\mathcal{P}(t) \propto \left(\frac{2}{q}\right)^t \times \prod_y \left(1 - \frac{1-|\langle Z_y\rangle|}{1+e^{y^2/2l(t)^2}}\right)^2. \tag{6}$$

This product has a relevant contributions only from a window of $|y| \lesssim \sqrt{t}$, hence it decays as $e^{-\gamma\sqrt{t}}$. Note that γ is larger when $|\langle Z_y\rangle|$ is smaller. By expanding each term in $e^{-y^2/2l(t)^2}$, we can approximate the product as $\approx e^{-\sqrt{2\pi}(1-|\langle Z\rangle|)l(t)}$, which is in good agreement with Monte Carlo results, at least away from $\langle Z\rangle \approx 0$ [33]. Note that Eq. (6) looks very similar to the probability of rare events from our heuristic argument in the simplest approximation of independently diffusing particles.

According to Eq. (6), in the large q limit $S_2^{(a)} = \log(q/2)t + a\sqrt{t}$, with $a \sim \mathcal{O}(1)$. Here, $\log(q/2)$ is exactly the large q limit of $v_E(q) = \log\frac{q+1/q}{2}$, the entanglement velocity of a non-symmetric random circuit with

q states per site [22, 23]. Moreover, the linear in t term is independent of the initial state. This suggests the following interpretation: there is an entanglement $v_{\rm E}(q)t$ coming entirely from non-conserved degrees of freedom, while the conserved spins are responsible for the $\propto \sqrt{t}$ term. This is supported by numerical results [33], which show that $S_2^{(a)}(t) - v_{\rm E}(q)t$ has only weak q-dependence and grows as $\sqrt{t}$ for any q, including the original model with $q = 1$, where $S_2^{(a)}$ is purely diffusive (Fig. 1a). This is true despite the ballistic spread of local operators in the symmetric circuit [29, 30], showing that recent arguments [20–22] for exponential decay of $\mathcal{P}$, based on the spreading of operators, fail in the present context, and subtle correlations between the spreading of different operators cannot be neglected. Our results also suggest that the 'minimal cut' picture of entanglement growth [18] does not accurately capture the behavior of $S_{\alpha\geq 2}$ [44].

Long-time tails.— Another scenario where diffusive modes have a strong influence is the long-time behavior of finite subsystems, which we turn to next. The entanglement eventually saturates to an equilibrium value predicted by the appropriate Gibbs ensemble, provided ETH holds and the initial state clusters [1, 3, 6, 7]. We now show that the approach to this thermodynamic value is also affected by diffusion and shows long-time hydrodynamic tails. Interestingly, we find that the precise nature of these tails depends strongly on the initial conditions, leading to the appearance of three different power laws, $t^{-1/2}$, t^{-1} and $t^{-3/2}$. In particular we uncover a difference between states at zero and finite chemical potential.

We take a spin 1/2 chain and rewrite the reduced density matrix of a small subsystem of l sites by inserting a complete basis of operators σ^μ, given by products of local Pauli operators acting on the subsystem, as in Ref. 20. This yields $S_2 = l\log 2 - \log\left(1 + \sum_\mu \langle\sigma^\mu\rangle^2\right)$, where the identity is excluded from the sum. To understand the approach to equilibrium, we write the expectation values as $\langle\sigma^\mu\rangle = \langle\sigma^\mu\rangle_{\rm eq} + \langle\delta\sigma^\mu\rangle$. At long times the distance from equilibrium is therefore proportional to

$$|\delta S_2| \equiv |S_2 - S_{2,\rm eq}| \propto \sum_\mu \left(2\langle\sigma^\mu\rangle_{\rm eq}\langle\delta\sigma^\mu\rangle + \langle\delta\sigma^\mu\rangle^2\right). \quad (7)$$

Thus the long-time tails that describe how expectation values equilibrate, appear directly in the Rényi entropy.

One immediate consequence of Eq. (7) is that the hydrodynamic tails can differ between states at half filling and away from half filling. At precisely half filling, the leading order term is $\langle\delta\sigma^\mu\rangle^2$, while away from half filling $\langle\sigma^\mu\rangle_{\rm eq}\langle\delta\sigma^\mu\rangle$ is expected to dominate. Generically, hydrodynamic observables should decay as $t^{-1/2}$ [26–28, 45], with subleading corrections $\mathcal{O}(t^{-3/4})$. Therefore, we generically expect a saturation as $\propto t^{-1}$ for states at half filling and $\propto t^{-1/2}$ otherwise. An analogous distinction between infinite and finite temperature states (respectively) holds for Hamiltonian systems. However, this expectation can change for certain initial states, where all hydrodynamic variables have $\langle\delta\sigma^\mu\rangle = 0$ initially. In this case one expects the leading diffusive tail to vanish and subleading corrections to take over. In particular, in the random circuit model one can argue [33] that the leading contribution for translation invariant product states should be of order $t^{-3/2}$.

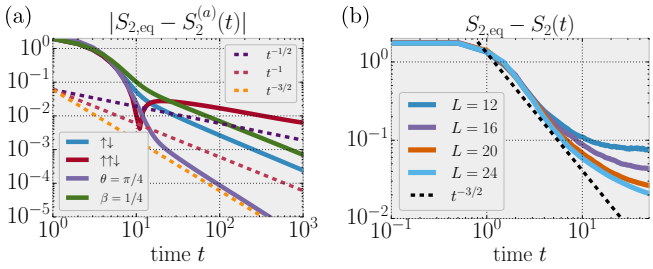

FIG. 3. Long-time tails in the saturation of the Rényi entropy. (a): saturation of $S_2^{(a)}$ for a 4-site subsystem in the spin 1/2 random circuit for different initial states. States away from half filling generically saturate as $t^{-1/2}$, and states at half filling as t^{-1}. Initial states where all hydrodynamic variables are in equilibrium at all times (see text) saturate with the subleading exponent $t^{-3/2}$. (b): The same $t^{-3/2}$ saturation is present for random product states in the tilted field Ising model (1) (3-site subsystem, averaged over 50 initial states).

We observe these three distinct power laws in $S_2^{(a)}$ for the spin 1/2 random circuit, as shown in Fig. 3a. We find that Néel-like states ($|\uparrow\uparrow\downarrow\uparrow\uparrow\downarrow\ldots\rangle$) with less then half filling exhibit an overshooting effect, approaching their equilibrium value *from above*, as $t^{-1/2}$. Finitely correlated states at half filling ($|\beta\rangle \propto e^{\beta\sum_{r=0}^{L-1} Z_r Z_{r+1}}(|\uparrow\rangle + |\downarrow\rangle)^{\otimes L}$) saturate as t^{-1}, and tilted ferromagnetic states ($|\theta\rangle \equiv e^{i\theta\sum_{r=1}^{L} Y_r}|\uparrow\rangle$) as $t^{-3/2}$. We also provide evidence of the $t^{-3/2}$ tail for random product states in the tilted field Ising Hamiltonian (1), shown in Fig. 3b.

Discussion.— Our results reveal a previously overlooked qualitative difference between the von Neumann and $\alpha \geq 2$ Rényi entropies. We gave a heuristic argument, indicating that the latter are strongly influenced by local quantum fluctuations which can lead to diffusive growth for the entropy in systems with diffusive transport. We presented evidence for this in two cases: a random circuit model and a thermalizing Hamiltonian. Our results indicate that diffusion leads to a separation of scales, where the half-chain density matrix contains a few largest eigenvalues that decay slowly and become well-separated from the bulk of the spectrum made up by exponentially small eigenvalues: S_2 is dominated by the former, while S_1 by the latter, such that they provide insight into different aspects of thermalization. [46].

We expect our results to generalize to higher dimensions. In that case the entanglement cut becomes a 'membrane' [17–19]. One can generate a 2D time evolution using a random circuit of 2-site gates [23], in which case

our Eq. (3) remains valid, with the membrane emitting Z_x operators that diffuse on the 2D lattice. A generalization of our heuristic argument would also suggest a similarly sub-ballistic growth for the Rényi entropy, but further work is needed to verify this explicitly. In particular, it would be interesting to see if effects like this could show up in holographic calculations, by extending the results of Ref. 19 and 47 to Rényi entropies.

It is an open question whether diffusion also affects S_1, either in the form of subleading corrections (we observe that the curve in Fig. 1d is not perfectly linear), or in long-time tails similar to the ones we discussed for S_2. Another avenue for future investigation is in the field of disordered systems, where even the von Neumann entropy is expected to grow sub-ballistically, while transport becomes sub-diffusive [48–50], eventually leading to many-body localization at strong disorder. Comparison of von Neumann and Rényi entropies could give further insight into the dynamics in these different regimes.

Acknowledgements. — We thank Michael Knap for useful comments. We are especially grateful to Adam Nahum for an illuminating discussion concerning the effect of rare events on entanglement growth. FP acknowledges the support of the DFG Research Unit FOR 1807 through grants no. PO 1370/2- 1, TRR80, the Nanosystems Initiative Mu- nich (NIM) by the German Excellence Initiative, and the European Research Council (ERC) under the European Unions Horizon 2020 research and innovation program (grant agreement no. 771537). CvK is supported by a Birmingham Fellowship.

[1] M. Rigol, V. Dunjko, and M. Olshanii, Nature **452**, 854 (2008).
[2] P. Calabrese and J. L. Cardy, Phys. Rev. Lett. **96**, 136801 (2006), arXiv:cond-mat/0601225 [cond-mat].
[3] L. D'Alessio, Y. Kafri, A. Polkovnikov, and M. Rigol, Advances in Physics **65**, 239 (2016), arXiv:1509.06411 [cond-mat.stat-mech].
[4] C. Gogolin and J. Eisert, Reports on Progress in Physics **79**, 056001 (2016).
[5] A. M. Kaufman, M. E. Tai, A. Lukin, M. Rispoli, R. Schittko, P. M. Preiss, and M. Greiner, Science **353**, 794 (2016), http://science.sciencemag.org/content/353/6301/794.full.pdf.
[6] J. M. Deutsch, Phys. Rev. A **43**, 2046 (1991).
[7] M. Srednicki, Phys. Rev. E **50**, 888 (1994).
[8] D. A. Abanin and E. Demler, Phys. Rev. Lett. **109**, 020504 (2012).
[9] A. J. Daley, H. Pichler, J. Schachenmayer, and P. Zoller, Phys. Rev. Lett. **109**, 020505 (2012).
[10] R. Islam, R. Ma, P. Preiss, M. Eric Tai, A. Lukin, M. Rispoli, and M. Greiner, (2015).
[11] A. Elben, B. Vermersch, M. Dalmonte, J. I. Cirac, and P. Zoller, Phys. Rev. Lett. **120**, 050406 (2018).
[12] P. Calabrese and J. Cardy, Journal of Statistical Mechanics: Theory and Experiment **2005**, P04010 (2005).
[13] P. Calabrese and J. Cardy, Journal of Statistical Mechanics: Theory and Experiment **2007**, P10004 (2007).
[14] V. Alba and P. Calabrese, Proceedings of the National Academy of Sciences **114**, 7947 (2017), http://www.pnas.org/content/114/30/7947.full.pdf.
[15] V. Alba and P. Calabrese, SciPost Phys. **4**, 17 (2018).
[16] H. Kim and D. A. Huse, Phys. Rev. Lett. **111**, 127205 (2013).
[17] A. Nahum, J. Ruhman, S. Vijay, and J. Haah, Phys. Rev. X **7**, 031016 (2017).
[18] C. Jonay, D. A. Huse, and A. Nahum, (2018), arXiv:1803.00089 [cond-mat.stat-mech].
[19] M. Mezei, Phys. Rev. D **98**, 106025 (2018).
[20] W. W. Ho and D. A. Abanin, Phys. Rev. B **95**, 094302 (2017).
[21] M. Mezei and D. Stanford, Journal of High Energy Physics **2017**, 65 (2017).
[22] C. W. von Keyserlingk, T. Rakovszky, F. Pollmann, and S. L. Sondhi, Phys. Rev. X **8**, 021013 (2018).
[23] A. Nahum, S. Vijay, and J. Haah, Phys. Rev. X **8**, 021014 (2018).
[24] T. Zhou and A. Nahum, (2018), arXiv:1804.09737 [cond-mat.stat-mech].
[25] B. Bertini, P. Kos, and T. Prosen, (2018), arXiv:1812.05090 [cond-mat.stat-mech].
[26] N. Bloembergen, Physica **15**, 386 (1949).
[27] P. D. Gennes, Journal of Physics and Chemistry of Solids **4**, 223 (1958).
[28] L. P. Kadanoff and P. C. Martin, Annals of Physics **24**, 419 (1963).
[29] V. Khemani, A. Vishwanath, and D. A. Huse, Phys. Rev. X **8**, 031057 (2018).
[30] T. Rakovszky, F. Pollmann, and C. W. von Keyserlingk, Phys. Rev. X **8**, 031058 (2018).
[31] F. Verstraete, V. Murg, and J. Cirac, Advances in Physics **57**, 143 (2008), https://doi.org/10.1080/14789940801912366.
[32] G. Vidal, Phys. Rev. Lett. **91**, 147902 (2003).
[33] See online supplemental material for details.
[34] More precisely, if the reduced density matrices of $|\phi_{0,1}\rangle$ on the left (right) half chain are $\rho^L_{0,1}$ ($\rho^R_{0,1}$), then we call them biorthogonal if $\mathrm{tr}(\rho^L_0\rho^L_1) = \mathrm{tr}(\rho^R_0\rho^R_1) = 0$.
[35] N. Linden, S. Popescu, and J. A. Smolin, Phys. Rev. Lett. **97**, 100502 (2006).
[36] C.-s. Yu, X. X. Yi, and H.-s. Song, Phys. Rev. A **75**, 022332 (2007).
[37] J. Niset and N. J. Cerf, Phys. Rev. A **76**, 042328 (2007).
[38] We have checked numerically that the same scaling applies also in the case of diffusing particles with hard core interactions, initiated in a Néel state.
[39] The heuristic argument clearly doesn't apply if there are some degrees of freedom in the systems that do not carry a conserved charge (see e.g. the finite q random circuit model below), which can be entangled without transporting charge across a bond. However, we do not expect this to be relevant for e.g. Hamiltonian systems, since in that case such degrees of freedom by definition do not appear in the Hamiltonian and are therefore static.
[40] The similarity of most apparent in the case of local *frustration free* Hamiltonians, where one can e.g. consider states that are ground states of all local terms within a region.
[41] M. B. Hastings, I. González, A. B. Kallin, and R. G.

Melko, Phys. Rev. Lett. **104**, 157201 (2010).
[42] P. Hayden, S. Nezami, X.-L. Qi, N. Thomas, M. Walter, and Z. Yang, Journal of High Energy Physics **2016**, 9 (2016).
[43] For example $Z_x \otimes \mathbb{1}$ is represented by a red particle on site x and $Z_{x+1} \otimes Z_{x+1}$ is represented by both a red and a blue particle on site $x+1$.
[44] This distinction between the entropies is consistent with results from holography, see also Ref. 19.
[45] J. Lux, J. Müller, A. Mitra, and A. Rosch, Phys. Rev. A **89**, 053608 (2014), arXiv:1311.7644 [cond-mat.quant-gas].
[46] Nevertheless, one could reconstruct the entire spectrum from full knowledge of all integer Rényi entropies with $\alpha \geq 2$. The information about the small eigenvalues is therefore 'hidden' in the subtle differences between different S_α.
[47] M. Mezei, Journal of High Energy Physics **2017**, 64 (2017).
[48] M. Žnidarič, A. Scardicchio, and V. K. Varma, Phys. Rev. Lett. **117**, 040601 (2016).
[49] D. J. Luitz, N. Laflorencie, and F. Alet, Phys. Rev. B **93**, 060201 (2016).
[50] A. Nahum, J. Ruhman, and D. A. Huse, Phys. Rev. B **98**, 035118 (2018).

Supplementary Material for "Sub-ballistic growth of Rényi entropies due to diffusion"

Appendix A: Circuit-averaged purity dynamics

We first re-derive the mapping from the random circuit model to an effective 'classical' description, originally described in Ref. 30, generalizing it to the model described in Ref. 29 in the process. This mapping provides the basis for an efficient method for calculating the average purity of the time evolved state, which we make us of in our numerical calculations. Furthermore, we take the $q \to \infty$ limit to arrive at the rules of the effective model presented in the main text.

We are interested in evolving operators that act on two copies of the original Hilbert space, which are relevant for evaluating the average purity. Time evolving such two-copy operators involves four instances of the time evolution operator U, therefore we require the fourth moment of each random gate, which can be evaluated in a relatively straightforward way. The result of averaging over a two-site gate is then a four-leg tensor. Each leg of this tensor in principle corresponds to $\mathcal{H}_1^{\otimes 4}$, where $\mathcal{H}_1$ is the one-site Hilbert space; however, in practice only a smaller dimensional subspace of this is relevant after averaging. Computing the average purity can then be achieved by contracting all these tensors together, which defines a two-dimensional tensor network, analogous to the calculation of the partition function of a 2D classical spin system. The boundary conditions of this partition function at times 0 and t depend on the initial state $\rho(0)$ and on the choice of the subsystem A, respectively.

We are interested in evaluating this partition function taking the on-site Hilbert space $\mathbb{C}^2 \otimes \mathbb{C}^q$ described in Ref. 29. In what follows Z_x denotes the local value of the conserved spin, which is an operator acting only on the $\mathbb{C}^2$ component of the on-site Hilbert space. It will not be necessary to construct an explicit operator basis for the $\mathbb{C}^q$ degrees of freedom. For arbitrary pairs of operators u, v, acting on a single site in the original Hilbert space $\mathbb{C}^2 \otimes \mathbb{C}^q$, we can assign the following operators acting on the doubled Hilbert space

$$\Lambda^-_{u|v} \equiv u \otimes v \qquad\qquad \Lambda^+_{u|v} \equiv (u \otimes v)\, \mathcal{F}, \tag{A1}$$

where $\mathcal{F} = \sum_{ij} e_{ij} \otimes e_{ji}$ is the on-site swap operator, where i is any on-site orthonormal basis. The tensor multiplication implicit in the second part of the above expressions is $(u \otimes v)(u' \otimes v') = uu' \otimes vv'$. The notion of Frobenius inner product between operators generalizes naturally to this two-copy space and yields

$$\langle \Lambda^\pm_{u|v} \mid \Lambda^\pm_{u'|v'} \rangle = \mathrm{tr}\left(u^\dagger u'\right) \mathrm{tr}\left(v^\dagger v'\right) \qquad\qquad \langle \Lambda^\mp_{u|v} \mid \Lambda^\pm_{u'|v'} \rangle = \mathrm{tr}\left(v^\dagger v' u^\dagger u'\right). \tag{A2}$$

The 'purity operator' for the half-chain containing sites $\leq x$ then reads $\mathcal{F}(x) \equiv \Lambda^{\leq x,+}_{1|1} \otimes \Lambda^{>x,-}_{1|1}$.

Consider now the effect of a two-site U(1)-symmetric unitary gate, acting on sites $x, x+1$. The two-site Hilbert space decomposes into three subspaces, labeled by the total charge $Q = 0, 1, 2$, corresponding to total spin-z components $+2, 0, -2$ respectively. Let P_Q denote the projector onto the two-site Hilbert spaces with charge $Q = 0, 1, 2$, which have dimension $d_Q = q^2, 2q^2, q^2$ respectively. Then averaging over four moments of the random gate yields an effective two-site evolution operator,

$$\overline{U^* \otimes U \otimes U^* \otimes U} \equiv \mathfrak{T}_{x,x+1} = \sum_{\sigma,\mu=\pm 1} \sum_{e_1 e_2} \frac{w_{\sigma\mu}(e_1, e_2)}{d_{e_1} d_{e_2} - \delta_{e_1 e_2}} \mid \Lambda^\sigma_{P_{e_1}|P_{e_2}} \rangle\langle \Lambda^\mu_{P_{e_1}|P_{e_2}} \mid \tag{A3}$$

where $w_+ = 1$ and $w_- = -\delta_{e_1 e_2} d_{e_1}^{-1}$. The terms appearing in this effective evolution are two-copy operators acting on the pair of sites $x, x+1$. In order to contract the tensor network one then needs to split them up to a sum of single-site two-copy operators, which in principle can be done in a many different ways, depending on the choice of local basis. Given such a local basis choice, the computation of the average purity reduces to contracting $2t$ layers of such two-site tensors, along with the boundary conditions defined by $\rho_0 \otimes \rho_0$ (where ρ_0 is the initial density matrix) and $\mathcal{F}(x)$. The contraction can be done in a variety of ways. In our numerical calculations we use a boundary MPS method [31], wherein the boundary tensors defined by $\mathcal{F}(x)$ are written as a matrix product state (MPS) and evolved layer-by-layer as in the Time Evolving Block Decimation (TEBD) algorithm [32]. Calculting the purity then amounts to taking the overlap of this time evolved MPS with another one that represents $\rho_0 \otimes \rho_0$. A further adventage of this method is that one can average over all product states analytically and incorporate the result into the boundary conditions, which yields the curve shown e.g. in Fig. 1a.

1. Large q limit

While Eq. (A3) yields an effective evolution that is numerically efficient, it is not analytically solvable, unlike the case of a random circuit without symmetries [50]. One can, however, simplify the equations by taking the $q \to \infty$ limit, which yields

$$\mathfrak{T}_{x,x+1}\left[\Lambda_{1|1}^{+,x} \otimes \Lambda_{1|1}^{-,x+1}\right] = \frac{2}{q} \times \frac{1}{2} \sum_{\sigma=\pm} \frac{1}{2}\left(\Lambda_{1|1}^{\sigma} + \Lambda_{Z_{x,x+1}|Z_{x,x+1}}^{\sigma}\right) + \mathcal{O}(q^{-3}). \tag{A4}$$

The terms $\Lambda^{\pm}_{Z_{x,x+1}|Z_{x,x+1}}$ are defined according to $Z_{x,x+1} = 2^{-1}(Z_x + Z_{x+1})$ and Eq. A1 and are identical to $\tilde{\mathcal{F}}_{x\mp1}(x\pm1)$ defined in the main text. Applied to the purity operator, the above equation then yields

$$\mathfrak{T}_{r,r+1}\left[\mathcal{F}(x)\right] = \delta_{x\neq r}\mathcal{F}(x) + \delta_{x,r}\frac{2}{q} \times \frac{1}{4}\sum_{\sigma}\left(\mathcal{F}(x+\sigma) + \sum_{z,w=x,x+1}\frac{1}{4}\mathcal{F}_{z,w}(x+\sigma)\right) + \mathcal{O}(q^{-3}). \tag{A5}$$

Here we have defined

$$\mathcal{F}_{\tau,\upsilon}(x) = \prod_i \Lambda_{Z_i^{\tau_i}|Z_i^{\upsilon_i}}^{(-1)^{\delta_{x<i}}}, \tag{A6}$$

$\tau_i, \upsilon_i = 0, 1$ indicate the positions of the z operators which we refer to as the positions of red and blue particles in the main text, as in Fig. 2c,d. x is the position of the cut. We have abbreviated a special case of such an operator with notation $\mathcal{F}_{y,z}(x)$ where x, y, z simply denote the position of the cut, and y, z are the positions at which a single τ, υ is nonzero. Eq. (A5) is exactly the result stated in Eq. (3). It is illustrated in terms of the red and blue particle picture in Fig. 4

Before moving on to derive equations of motion for these operators, let us try to gain some intuition about their physical meaning. When evaluated in a pure state they give, focusing on the simplest case ...

$$\langle\tilde{\mathcal{F}}_{x-1}(x)\rangle \equiv \langle\tilde{\mathcal{F}}_{x-1}(x) \mid \rho\otimes\rho\rangle = \left|\left|\mathrm{tr}_{\leq x}\left(\hat{P}_0^{x-1,x}\rho - P_2^{x-1,x}\rho\right)\right|\right|^2, \tag{A7}$$

where $P_Q^{x-1,x}$ is a projector that projects onto eigenstates of the two-site charge operator $\hat{Q}_{x-1,x}$ with eigenvalue Q. This expression is a direct measure of how distinguishable the positive matrices $\hat{P}_0\rho\hat{P}_0$ and $\hat{P}_2\rho\hat{P}_2$ are through measurements purely on the subsystem consisting of sites to the right of x. It is therefore directly related to local quantum fluctuation of the charge density on these two sites. In particular they are sensitive to the sort of 'rare configurations' discussed in our heuristic argument, where the neighborhood of the entanglement cut if completely empty/filled.

To find the equations of motion for the terms $\mathcal{F}_{\tau,\upsilon}(y)$, it is necessary and sufficient to determine the dynamics of various two site operators of form $\Lambda_{a|b}^{\pm,x} \otimes \Lambda_{a'|b'}^{\pm,x+1}$ and $\Lambda_{a|b}^{\pm,x} \otimes \Lambda_{a'|b'}^{\mp,x+1}$ where $a, b, a', b = 1, Z'$. To begin, the following operators are exactly invariant under $\mathfrak{T}_{x,x+1}$

$$\Lambda_{1|1}^{\pm,x} \otimes \Lambda_{1|1}^{\pm,x+1} \qquad \Lambda_{Z_x|1}^{\pm,x} \otimes \Lambda_{Z_{x+1}|1}^{\pm,x+1} \qquad \Lambda_{1|Z_x}^{\pm,x} \otimes \Lambda_{1|Z_{x+1}}^{\pm,x+1} \qquad \Lambda_{Z_x|Z_x}^{\pm,x} \otimes \Lambda_{Z_{x+1}|Z_{x+1}}^{\pm,x+1},$$

These correspond to the statement that, far away from the cut, there are no dynamics for red (blue) particles if the pair of sites in question are empty or fully occupied with red (blue) particles.

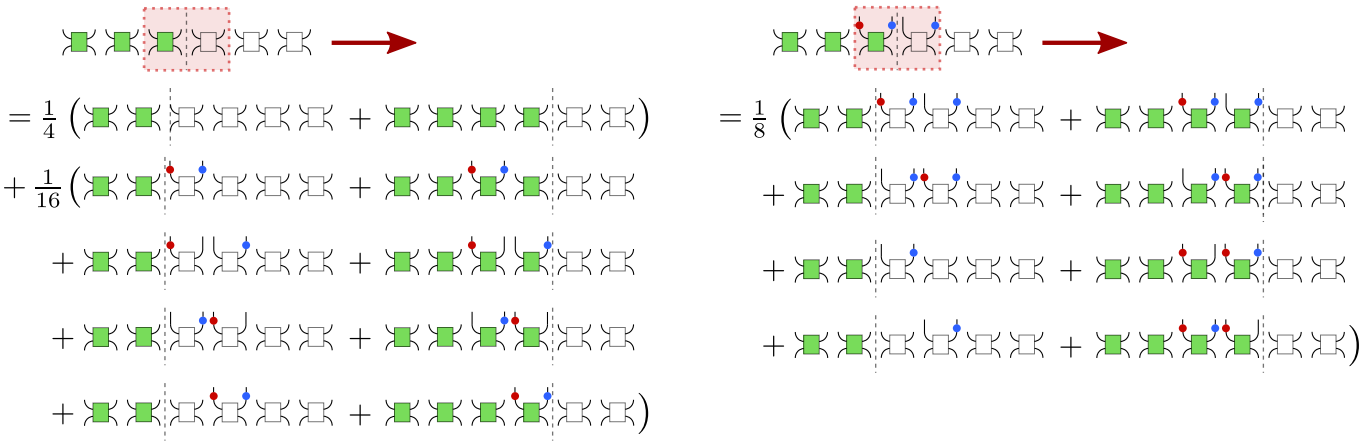

FIG. 4. Illustration of some of the two-site update rules in the large q effective model. Left: evolution of a swap-string, given by Eq. (A5). The two-site gate (red dotted line) moves the string by one site, while producing spin-operators on both copies of the Hilbert space, denoted by red and blue particles respectively. Right: evolution o a more complicated configuration, with several particles already present near the endpoint of the string.

The following superoperators have very simple evolutions under $\mathfrak{T}_{x,x+1}$ which follow immediately from Haar averaging.

$$\begin{aligned}
\Lambda^{\pm,x}_{Z_x|1}\otimes\Lambda^{\pm,x+1}_{1|1},\Lambda^{\pm,x}_{1|1}\otimes\Lambda^{\pm,x+1}_{Z_{x+1}|1}&\to\frac{1}{2}\left(\Lambda^{\pm,x}_{Z_x|1}\otimes\Lambda^{\pm,x+1}_{1|1}+\Lambda^{\pm,x}_{1|1}\otimes\Lambda^{\pm,x+1}_{Z_{x+1}|1}\right)\\
\Lambda^{\pm,x}_{1|Z_x}\otimes\Lambda^{\pm,x+1}_{1|1},\Lambda^{\pm,x}_{1|1}\otimes\Lambda^{\pm,x+1}_{1|Z_{x+1}}&\to\frac{1}{2}\left(\Lambda^{\pm,x}_{1|Z_x}\otimes\Lambda^{\pm,x+1}_{1|1}+\Lambda^{\pm,x}_{1|1}\otimes\Lambda^{\pm,x+1}_{1|Z_{x+1}}\right)\\
\Lambda^{\pm,x}_{Z_x|Z_x}\otimes\Lambda^{\pm,x+1}_{1|Z_{x+1}},\Lambda^{\pm,x}_{1|Z_x}\otimes\Lambda^{\pm,x+1}_{Z_{x+1}|Z_{x+1}}&\to\frac{1}{2}\left(\Lambda^{\pm,x}_{Z_x|Z_x}\otimes\Lambda^{\pm,x+1}_{1|Z_{x+1}}+\Lambda^{\pm,x}_{1|Z_x}\otimes\Lambda^{\pm,x+1}_{Z_{x+1}|Z_{x+1}}\right)\\
\Lambda^{\pm,x}_{Z_x|Z_x}\otimes\Lambda^{\pm,x+1}_{Z_{x+1}|1},\Lambda^{\pm,x}_{Z_x|1}\otimes\Lambda^{\pm,x+1}_{Z_{x+1}|Z_{x+1}}&\to\frac{1}{2}\left(\Lambda^{\pm,x}_{Z_x|Z_x}\otimes\Lambda^{\pm,x+1}_{Z_{x+1}|1}+\Lambda^{\pm,x}_{Z_x|1}\otimes\Lambda^{\pm,x+1}_{Z_{x+1}|Z_{x+1}}\right)
\end{aligned}$$

We also meet more four more involved products

$$\begin{aligned}
\Lambda^{\pm,x}_{Z_x|Z_x}\otimes\Lambda^{\pm,x+1}_{1|1},\Lambda^{\pm,x}_{1|1}\otimes\Lambda^{\pm,x+1}_{Z_{x+1}|Z_{x+1}}&\to\Lambda^{\pm}_{Z_{x,x+1}|Z_{x,x+1}}+\frac{1}{2q^2}\Lambda^{\mp}_{\frac{1-Z_xZ_{x+1}}{2}|\frac{1-Z_xZ_{x+1}}{2}}+\mathcal{O}_{\rm rel}(q^{-4})\\
\Lambda^{\pm,x}_{Z_x|1}\otimes\Lambda^{\pm,x+1}_{1|Z_{x+1}},\Lambda^{\pm,x}_{1|Z_x}\otimes\Lambda^{\pm,x+1}_{Z_{x+1}|1}&\to\Lambda^{\pm}_{Z_{x,x+1}|Z_{x,x+1}}-\frac{1}{2q^2}\Lambda^{\mp}_{\frac{1-Z_xZ_{x+1}}{2}|\frac{1-Z_xZ_{x+1}}{2}}+\mathcal{O}(q^{-4}).
\end{aligned}$$

The $O(q^{-2})$ terms on the second line are subleading, and introduce a new entanglement cut at the next time step, which will accrue additional suppressing $O(q^{-1})$ factors; we henceforth ignore these terms. The above 16 mappings reflect the statement that, far from the cut and at leading order, red and blue particles undergo single-file diffusion.

We have listed all the possible products on one site of a cut. Finally we meet products involving sites near the entanglement cut, such as

$$\begin{aligned}
\Lambda^{\pm,x}_{1|1}\otimes\Lambda^{\mp,x+1}_{1|1}&\to\frac{2}{q}\times\frac{1}{2}\sum_{\sigma=\pm}\frac{1}{2}\left(\Lambda^{\sigma}_{1|1}+\Lambda^{\sigma}_{Z_{x,x+1}|Z_{x,x+1}}\right)+O(q^{-3})\\
\Lambda^{\pm,x}_{Z_x|1}\otimes\Lambda^{\mp,x+1}_{Z_{x+1}|1}&\to\frac{2}{q}\times\frac{1}{2}\sum_{\sigma=\pm}\frac{1}{2}\left(\Lambda^{\sigma}_{Z_xZ_{x+1}|1}+\Lambda^{\sigma}_{Z_{x,x+1}|Z_{x,x+1}}\right)+O(q^{-3})\\
\Lambda^{\pm,x}_{1|Z_x}\otimes\Lambda^{\mp,x+1}_{1|Z_{x+1}}&\to\frac{2}{q}\times\frac{1}{2}\sum_{\sigma=\pm}\frac{1}{2}\left(\Lambda^{\sigma}_{1|Z_xZ_{x+1}}+\Lambda^{\sigma}_{Z_{x,x+1}|Z_{x,x+1}}\right)+O(q^{-3}).
\end{aligned}$$

The first mapping above shows that the cut can create red and blue particles from nothing in pairs, and is indeed equivalent to Eq. A5. The second and third equation shows that the particles created can correlate with the direction of motion of the cut. We have further related equations showing that the cut can scatter a red to a blue particle and

vice versa:

$$\Lambda^{\pm,x}_{Z_x|1}\otimes\Lambda^{\mp,x+1}_{1|1},\Lambda^{\mp,x}_{1|1}\otimes\Lambda^{\pm,x+1}_{Z_{x+1}|1}\to\frac{2}{q}\frac{1}{4}\left(\Lambda^{\pm}_{Z_{x,x+1}|I}+\Lambda^{\pm}_{Z_xZ_{x+1}|Z_{x,x+1}}+\Lambda^{\mp}_{Z_{x,x+1}|I}+\Lambda^{\mp}_{I|Z_{x,x+1}}\right)+O(q^{-3})$$

$$\Lambda^{\pm,x}_{1|Z_x}\otimes\Lambda^{\mp,x+1}_{1|1},\Lambda^{\mp,x}_{1|1}\otimes\Lambda^{\pm,x+1}_{1|Z_{x+1}}\to\frac{2}{q}\frac{1}{4}\left(\Lambda^{\pm}_{I|Z_{x,x+1}}+\Lambda^{\pm}_{Z_{x,x+1}|Z_xZ_{x+1}}+\Lambda^{\mp}_{I|Z_{x,x+1}}+\Lambda^{\mp}_{Z_{x,x+1}|I}\right)+O(q^{-3})$$

Note also that

$$\Lambda^{\pm,x}_{Z_x|Z_x}\otimes\Lambda^{\mp,x+1}_{1|1},\Lambda^{\mp,x}_{1|1}\otimes\Lambda^{\pm,x+1}_{Z_{x+1}|Z_{x+1}}\to\frac{2}{q}\frac{1}{4}\left(\Lambda^{\pm}_{Z_xZ_{x+1}|Z_xZ_{x+1}}+\Lambda^{\pm}_{Z_{x,x+1}|Z_{x,x+1}}+\Lambda^{\mp}_{1|1}+\Lambda^{\mp}_{Z_{x,x+1}|Z_{x,x+1}}\right)+O(q^{-3})$$

$$\Lambda^{\pm,x}_{Z_x|1}\otimes\Lambda^{\mp,x+1}_{1|Z_{x+1}},\Lambda^{\mp,x}_{1|Z_x}\otimes\Lambda^{\pm,x+1}_{Z_{x+1}|1}\to\frac{2}{q}\frac{1}{4}\left(\Lambda^{\pm}_{Z_xZ_{x+1}|1}+\Lambda^{\pm}_{Z_{x,x+1}|Z_{x,x+1}}+\Lambda^{\mp}_{1|Z_xZ_{x+1}}+\Lambda^{\mp}_{Z_{x,x+1}|Z_{x,x+1}}\right)+O(q^{-3})$$

the first of which shows that the cut can destroy particles in pairs as well. Finally

$$\Lambda^{\pm,x}_{Z_x|Z_x}\otimes\Lambda^{\mp,x+1}_{Z_{x+1}|Z_{x+1}}\to\frac{2}{q}\times\frac{1}{2}\sum_{\sigma=\pm}\frac{1}{2}\left(\Lambda^{\sigma}_{Z_xZ_{x+1}|Z_xZ_{x+1}}+\Lambda^{\sigma}_{Z_{x,x+1}|Z_{x,x+1}}\right)+O(q^{-3})$$

$$\Lambda^{\pm,x}_{Z_x|Z_x}\otimes\Lambda^{\mp,x+1}_{Z_{x+1}|1},\Lambda^{\mp,x}_{Z_x|1}\otimes\Lambda^{\pm,x+1}_{Z_{x+1}|Z_{x+1}}\to\frac{2}{q}\frac{1}{4}\left(\Lambda^{\pm}_{Z_xZ_{x+1}|Z_{x,x+1}}+\Lambda^{\pm}_{Z_{x,x+1}|Z_xZ_{x+1}}+\Lambda^{\mp}_{Z_xZ_{x+1}|Z_{x,x+1}}+\Lambda^{\mp}_{Z_{x,x+1}|I}\right)+O(q^{-3})$$

$$\Lambda^{\pm,x}_{Z_x|Z_x}\otimes\Lambda^{\mp,x+1}_{1|Z_{x+1}},\Lambda^{\mp,x}_{1|Z_x}\otimes\Lambda^{\pm,x+1}_{Z_{x+1}|Z_{x+1}}\to\frac{2}{q}\frac{1}{4}\left(\Lambda^{\pm}_{Z_{x,x+1}|Z_xZ_{x+1}}+\Lambda^{\pm}_{Z_xZ_{x+1}|Z_{x,x+1}}+\Lambda^{\mp}_{Z_{x,x+1}|Z_xZ_{x+1}}+\Lambda^{\mp}_{I|Z_{x,x+1}}\right)+O(q^{-3})$$

Note that each of the last 16 terms involves the action of the circuit in the vicinity of the cut, and are correspondingly suppressed by a factor of $2/q$. Otherwise, these equations exhibit a rich set of behaviors. For example, the cut can create and absorb particles in pairs, and can convert a red particle to a blue particle and vice versa. The cut itself always appears to have an equal chance of moving to the left or right although its motion can correlate with changes to the red/blue populations.

The full set of two site calculations above show that, up to $O(q^{-2})$ corrections, the Haar averaged dynamics are closed in the space of operators spanned by $\mathcal{F}_{\tau,\upsilon}(x)$ (see Eq. A6) where τ,υ denote the possible configurations of red and blue particles alluded to in the text. Moreover, saving for the overall factor of $2/q$ at each global time step, the induced dynamics on this restricted space of operators is in fact Markovian leading to a stochastic process on the configuration space of cuts and blue and red particle configurations $\{x,\{\tau_y\},\{\upsilon_y\}\}$; i.e., ignoring the $2/q$ factor, the RHS coefficients in all the mappings listed below Eq. A7 add up to unity.

Appendix B: Entanglement growth for various initial states

Here we complement the results presented in the main text, where we averaged over different initial product states, with further data on various initial states. We start by considering the U(1) symmetric random circuit at different values of q and show that the annealed average entropy, $S_2^{(a)}$, behaves similarly for the different states defined around Eq. (7) in the text.

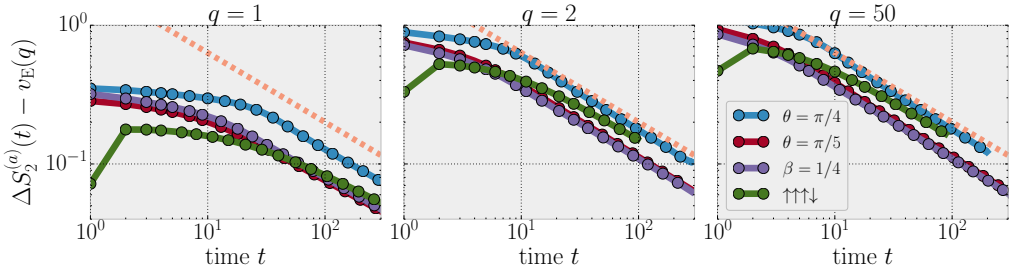

FIG. 5. Time derivative of the annealed average Rényi entropy in the random circuit at different values of q, after subtracting the constant term, $v_E(q)$, associated to the non-conserved degrees of freedom. All states show a decay of the form $\propto t^{-1/2}$ at long times, indicating diffusive growth.

In the spin 1/2 circuit, our results are consistent with the predicted $\propto\sqrt{t}$ growth of the Rényi entropy for all all initial states. The same is true at finite q after subtracting the linear $v_E(q)t$ term coming from the additional degrees

of freedom that do not carry any conserved charge. This is shown in Fig. 5. We find that the times needed for Néel-like states to cross-over to sub-ballistic growth are longer then the time scales for other states that are not global eigenstates of the conserved quantity. This is in agreement with our heuristic argument, presented in the main text: the rare events leading to slow growth are already present for the latter states, while they have to be dynamically generated in the former.

Note that after subtracting $v_E t$ from the entanglement, there are only small differences between the curves for different q (especially for $q \geq 2$). This further reinforces our interpretation that we can associate this quantity primarily to the conserved spins, and that we are justified in extrapolating the analytical results of the $q = \infty$ model back to $q = 1$.

We also consider the tilted field Ising model for a particular initial product state. To have a state which is both translation invariant and corresponds to infinite temperature, we take a state which is an eigenstate of the Y Pauli operator on each site with an eigenvalue $+1$. Since both the state and the dynamics are translation invariant, we can time evolve directly in the thermodynamic limit, utilizing the infinite time-evolving block decimation (iTEBD) algorithm [32]. The times obtainable are then limited by the maximal bond dimension χ. We find a behavior analogous to the one observed for random product states in the main text: S_1 grows approximately linearly, while S_∞ curves over to an approximately diffusive growth at times $t \approx 10$ (left panel of Fig. 6). One way to think about this phenomenon is as a separation of scales in the spectrum of the reduced density matrix, whose largest eigenvalues decay as $\Lambda_i \sim e^{-\sqrt{t}}$, while the majority of the eigenvalues are exponentially small, $\Lambda_i \sim e^{-t}$ (right panel of Fig. 6).

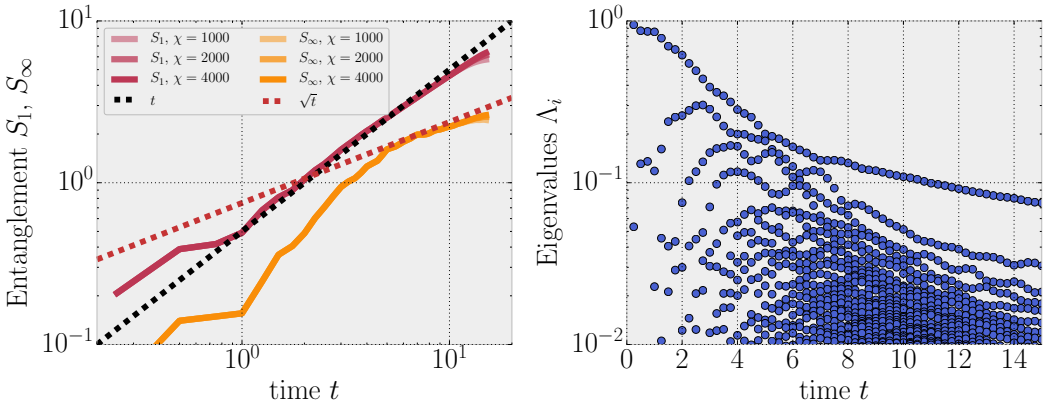

FIG. 6. Entanglement growth in the tilted field Ising model, starting from an initial state polarized in the positive Y direction, evolved with the iTEBD algorithm at various bond dimensions χ. We observe a cross-over to sub-ballistic growth in the min-entropy S_∞, as opposed to S_1, which remains ballistic (left). This shows up in the spectrum of the half-chain reduced density matrix, where the largest eigenvalue is separated from the bulk of the spectrum at long times (right).

Appendix C: Hydrodynamic tails in the spin 1/2 random circuit

In this section we describe the behavior of various correlation functions in the U(1) conserving random circuit model, lifting intuition from random circuit calculations performed previously in Refs. 29 and 30. Our results are in line with the standard lore of hydrodynamics: the space of local observables splits into an orthogonal sum of hydrodynamic and non-hydrodynamic variables. In a short range correlated initial state, the former can decay according to a power law at long times and have diffusive spatiotemporal behavior, while the latter always decay exponentially quickly. An advantage of our approach, compared to the usual scaling arguments [45], is that we are able to make statements about the differences in behavior for different homogenous initial states; something we expect to be of independent interest.

We start with an exact rewriting of the circuit evolved Z_r operator

$$Z_r(t) = D_r(t) + B_r(t), \tag{C1}$$

where $D_r(t) = \sum_{r'} K_{rr'}(t) Z_{r'}$ and $K_{rr'}(t)$ is a lattice diffusion kernel, and where

$$B_r(t) = \frac{1}{2} \sum_{\tau=1}^{t} \sum_{x=\tau \mod 2} (\partial_x K_{rx}(\tau)) \Gamma_x(t;\tau), \tag{C2}$$

State	$\overline{\langle \delta Z_r \rangle}$	$\overline{\langle \delta Z_r \rangle \langle \delta Z_s \rangle}$	$\overline{\delta(\langle Z_r Z_s \rangle)}$	$\lvert \delta S_2 \rvert$
$\uparrow\downarrow$	$O(e^{-\pi^2 t/2})$	$O(t^{-3/2})$	$O(t^{-1/2})$	$O(t^{-1})$
$\uparrow\uparrow\downarrow$	$O(e^{-\pi^2 t/3})$	$O(t^{-3/2})$	$O(t^{-1/2})$	$O(t^{-1/2})$
θ-state	0	$O(t^{-3/2})$	0	$O(t^{-3/2})$
β-state	0	$O(t^{-3/2})$	$O(t^{-1/2})$	$O(t^{-1})$

TABLE I. Summary of the saturation behavior of various circuit averaged correlation functions, their moments and the Rényi entropy at large times $t \gg |r-s|^2$ in the spin 1/2 random circuit.

with $\Gamma_x(t;\tau) \equiv (Z_x - Z_{x+1})(t;\tau)$. No approximations have been made thus far. The operator weight in D_r is $\sum_{r'} K_{rr'}^2 = O(t^{-1/2})$, while that in B_r is $1 - O(t^{-1/2})$ [29, 30]. We will assume that $\Gamma_x(t;\tau)$ grows ballistically, so that it is effectively a random superposition of operators of typical radius $v_B(t-\tau)$. This assumption can only be an approximation to the full story, in part because $Z_x - Z_{x+1}$ is itself a hydrodynamical variable. However, it turns out that the expectation values of this tail is either exactly zero (θ-states) or decays exponentially in time (Néel-like states), so we are justified in ignoring it.

In considering the growth of fluctuations, we also consider operators of the form $Z_r(t)Z_s(t)$. These we may similarly write exactly as

$$Z_r(t)Z_s(t) = \sum_{r's'} K_{rs}^{r's'}(t) Z_{r'} Z_{s'} + B_{rs}(t). \tag{C3}$$

The random circuit calculation demonstrates that, under averaging, the two operators engage in single file diffusion, which we take to have kernel $K_{rs}^{r's'}(t)$. $B_{rs}(t)$ is again assumed to be a ballistically spreading and effectively random superposition of operators. In the following we explain how to estimate the various correlation functions presented in Table I, using operator spreading intuition.

One point functions The average behavior of $\langle Z_r(t) \rangle$ is simple to compute for various states through substitution of Eq. C1. This leads to two expressions $\langle D_r(t) \rangle$ and $\langle B_r(t) \rangle$. The former is independent of time for translation invariant states, and determined by the filling, while for the Neel state it decays exponentially with t because $\sum_{r'} (-1)^{r'} K_{rr'}(t) \sim e^{-\frac{\pi^2 t}{2}}$. The B_r term is more involved, but on average expected to be zero because $\Gamma_x(t;\tau)$ is a superposition of operators with random signs.

Fluctuations in one point functions The average behavior of $\overline{\langle Z_r(t) \rangle \langle Z_s(t) \rangle}$ can also be computed using C1. Using the results in the previous paragraph, two terms survive the noise averaging, $\langle D_r(t) \rangle \langle D_s(t) \rangle$ and $\overline{\langle B_r(t) \rangle \langle B_s(t) \rangle}$. The former term can be calculated using the paragraph above, while the latter require a more involved discussion. Using

$$\overline{\langle B_r(t) \rangle \langle B_s(t) \rangle} = \frac{1}{2} \sum_{,\tau'\tau=1}^{t} \sum_{x,y=\tau \mod 2} \partial_x K_{rx}(\tau) \partial_y K_{sy}(\tau) \overline{\langle \Gamma_x(t;\tau) \rangle \langle \Gamma_y(t;\tau) \rangle} \tag{C4}$$

To approximate this sum, we first note that, as $\Gamma_y(t;\tau)$ tends to grow ballistically, its expectation value on a short range correlated state will tend to decay exponentially quickly (a string of operators of length R has a typical expectation value $e^{-\alpha R}$ on a product state). So the sum is dominated by τ, τ' near t. Moreover, due to the spatial randomness of the circuit, the sign of the expectation values $\langle \Gamma_{x/y}(t;\tau) \rangle$ are uncorrelated unless $x = y$. Hence we approximate Eq. C4 by restricting the sum to $\tau', \tau = t-1, x = y$. At large times $t \gg |r-s|^2/D$, the distinction between r, s becomes unimportant, and the contribution goes as $\int dx \, (\partial_x K_{rx})^2 \sim t^{-3/2}$.

Two point functions In order to compute $\overline{\langle Z_r(t) Z_s(t) \rangle}$ we substitute in Eq. C3 and assume the ballistic terms source random signs that cancel on averaging. This leads to precisely one contribution $\sum_{r's'} K_{rs}^{r's'}(t) \langle Z_{r'} Z_{s'} \rangle$ where $K_{rs}^{r's'}(t)$ is the single file lattice diffusion propagator. This is independent of time for translation invariant states, but remarkably is found to decay as $\sim \frac{1}{\sqrt{t}}$ for the Neel state. In the case of ϵ states we substitute $\langle Z_{r'} Z_{s'} \rangle \sim e^{-|r'-s'|/\xi}$; for finite ϵ, this will have the effect of restricting $|r'-s'| \leq \xi$ in the sum above. The leading behavior is obtained by setting $r' = s'$, which gives $\sum_{r'} K_{rs}^{r'r'}(t) \sim t^{-1/2}$.